INVESTIGATION OF METAL-SEMICONDUCTOR CONTACTS ON MOS2 AND ITS HETEROJUNCTION WITH GAN FOR PHOTODETECTOR APPLICATIONS

MONIKA

DEPARTMENT OF PHYSICS
INDIAN INSTITUTE OF TECHNOLOGY DELHI

JULY 2020

©Indian Institute of Technology Delhi (IITD), New Delhi, 2020

Investigation of Metal-Semiconductor Contacts on MoS_2 and its Heterojunction with GaN for Photodetector Applications

by

Monika

Department of Physics

Submitted

in fulfillment of the requirements of the degree of Doctor of Philosophy

to the

INDIAN INSTITUTE OF TECHNOLOGY DELHI

July 2020

Certificate

This is to certify that the thesis entitled **"Investigation of Metal-Semiconductor Contacts on MoS_2 and its Heterojunction with GaN for Photodetector Applications"** being submitted by **Ms. Monika** to **Indian Institute of Technology Delhi** for the award of the degree of **Doctor of Philosophy** is a record of bonafide research work carried out by her. She has worked under my guidance and supervision and has fulfilled the requirements, which to our knowledge have reached the requisite standard for the submission of the thesis.

The results contained in this thesis have not been submitted in part or full to any other University or Institute for the award of any degree or diploma.

Date:
NEW DELHI

Prof. Rajendra Singh
Department of Physics
Indian Institute of Technology Delhi
New Delhi- 110016
INDIA

Acknowledgements

My PhD time at IIT Delhi has been challenging and enjoyable but more life defining. I learnt a lot during my course from my professors, lab mates, colleagues and friends. I would like to thank them all for their support, criticism, inspiration that helped me to change myself for betterment.

First of all, I would like to express my sincere gratitude to my PhD supervisor Prof. Rajendra Singh. It has been an honor for me to be his student. I am grateful to him for his useful suggestions, encouragements to work on research ideas and providing opportunity to do experimental work. I learnt a lot under his supervision and tried to improve myself considering his suggestions. I appreciate him for giving his useful time, discuss problems, and most importantly, pushing me and believing in me.

I would also like to thank my PhD research committee members Prof. Sujeet Chaudhary, Prof. J.P. Singh and Prof. M. Jagadesh Kumar for their timely evaluations, comments and suggestions during the course of research work. I acknowledge the department of Physics, Indian Institute of Technology Delhi for giving me the opportunity to work here.

I acknowledge University Grants Commission (UGC) for providing research fellowship. I am also grateful to Indian Institute of Technology Delhi and the department of Science and technology (DST) for providing me funding to attend international conferences outside India.

I express my deep gratitude towards Dr. Subramaniyam Nagarajan, Aalto University, Finland for providing MOVPE grown GaN samples. I gratefully acknowledge Dr. Suchandan Pal and Vipul Pandey, Central Electronics Engineering Research Institute (CEERI) Pilani for bilayer Ohmic contact metallization and Rapid Thermal Annealing of the metal contacts. I am also thankful to Dr. Priyanka Periwal with whom I started my research work. I gratefully acknowledge the Nanoscale Research Facility (NRF) centre at Indian Institute of Technology Delhi for providing experimental facilities during this course of work.

I am grateful to Prof. Chennupati Jagadish, Prof. Hoe Tan at Australian National University (ANU) for giving me the opportunity to do some experiments in their labs. I also acknowledge Dr. Fouad

Karouta, Dr. Kaushal Vora, Mr Dipankar Chugh and Mr Sonachand for helping me in carrying out the experiments.

Working at Advanced Semiconductor Materials, Nanostructures and Devices Laboratory, IIT Delhi, has been an enriching experience. I would like to thank my seniors Dr. Uday Dadwal, Dr. Ashutosh Kumar, Dr. Sudheer Kumar, Dr. Mukesh Kumar, Dr. Chandra Shekhar Pathak and Dr. Manjari Garg for their valuable suggestions and help. I also express my gratitude to my colleagues Ravi Pathak, Chandan Sharma, Bhera Ram Tak, Aditya Singh, Kapil Narang, Shuchi Kaushik, Sahin Sorifi, Madan Pancholi, Hardhyan, Pallavi Agarwal, Prithu Bhatnagar, Kalyani Thakur, Anjali Chauhan, Aarti, Sukhdeep Gill, Mohd. Danish Ali, Swapnil and Arun for scientific and personal discussions. Once again, I thank all these members for making my stay at IIT Delhi, unforgettable.

I will never forget my friends at IIT Delhi without whom this PhD would have been more challenging. I would like to thank Parul Raturi, Hemlata, Pratiksha Gangwar. Rupali Das, Pragati Aashna for spending good times. Also, excursions and dinners with Manjari Garg, Ravi Pathak, Bhera Ram Tak and Aditya Singh will be treasured.

Finally, words are inadequate to express my deep gratitude towards my family for their blessings, unconditional love, care, support, encouragement, patience and sacrifices during all the stages of my PhD. I would be nothing without my family and I thank them to be with me in both good and bad times. Thank you.

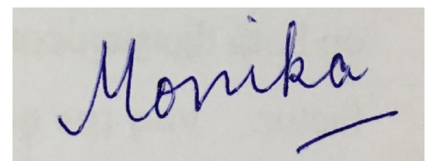

Monika

Abstract

Molybdenum disulfide (MoS_2), a layered transition metal dichalcogenide has shown its potential in nanoelectronics due to its layer dependent unique properties. One of the unique features of MoS_2 is the bandgap transition from indirect to direct as the layer number decreases to single atomic layer. Various electronic devices based on MoS_2 have been demonstrated such as FETs, photodetectors, sensors, flexible and transparent devices etc. reflecting its potential in modern device world. Performance of the electronic devices are primarily governed by metal-semiconductor contacts and the fabrication of high quality electrical contacts to MoS_2 becomes crucial for proper functioning of the device. We set our first aim to realize optimal electrical contacts on MoS_2 and determine the dominant current transport mechanism at the interface. Considering the monolayer counterpart of MoS_2, its direct bandgap nature, high electrical performance even in ultrathin form makes it suitable material for applications in small sized optoelectronic devices. As our second aim, we try to investigate the photodetection phenomenon in monolayer MoS_2 device. Besides devices based on only MoS_2, its heterojunction with other conventional materials have gained significant amount of research attention. Existence of van der Waals forces in layered materials open opportunities to demonstrate various combination of heterostructures as compared to other traditional methods for growth of heterostructures. Next, we aim at the demonstration of heterostructures device design based on MoS_2 and gallium nitride (GaN). The heterojunction devices enhance the functionality of both semiconductors and could lead to new device applications.

In the initial part of the work, the electrical contacts were fabricated and characterized on mechanically exfoliated MoS_2 flakes. Comparative electrical study on MoS_2 was performed with different metals and the current-voltage characteristics reveal that silver shows 2 orders of higher current and better linearity and symmetry of I-V curves than other metals such as nickel and chromium contacts. Formation of Ohmic contact can't be confirmed only by linear behavior of the current-voltage curve. Therefore, transmission line model (TLM) was applied using Ag/Au contacts on MoS_2. Specific contact resistivity is measured to be 4.54×10^{-4} Ω–cm^2. Further, Pt/MoS_2 Schottky barrier diode was fabricated with a high rectification ratio of about 900. Barrier

height and ideality factor of 0.56 eV and 2.1, respectively have been obtained using thermionic emission current equations. Next, temperature-dependent electrical characterizations of microscopic Pt/MoS_2 Schottky diode were performed. Rectifying current-voltage characteristics were obtained in the whole temperature range from room temperature to 80 K. As temperature decreases from 296 K to 80 K, Schottky barrier height decreases whereas ideality factor increases. The temperature dependence of Schottky diode parameters was explained on the basis of barrier inhomogeneity model. Assuming the Gaussian distribution of Schottky barrier height, the inhomogeneity level was found to be 64 and 102 meV in the temperature regions 80 K to 140 K and 160 K to 296 K, respectively. These observations show the inhomogeneous Schottky barrier even in microscale devices.

In the subsequent work, optoelectronic performance of monolayer MoS_2 was studied as it is a direct bandgap semiconductor. Pd/MoS_2/Pd metal-semiconductor-metal geometry was opted to make high barrier photodetector on MoS_2. Electrical characterizations reveal high Schottky barrier present at Pd-MoS_2 interface leading to low dark current. The device exhibits significant current enhancement after illumination with the responsivity of 0.8 A/W at power density of 2 mW/cm^2 for 650 nm laser. The linear behavior of photocurrent with incident power density reveals less effect of trap states on the performance of the MSM device. Responsivity was also observed to enhance with the increasing laser power density. The photodetection performance of the device was also examined at higher temperatures to check device stability. The optoelectronic performance of the fabricated device was examined by current measurement at higher operating temperatures. Photodetector parameters such as photo to dark current ratio (PDCR) and responsivity were observed to vary with temperature. PDCR was observed to decrease whereas responsivity was observed to enhance with increase in temperature. The increase in dark current as well as photocurrent at higher temperatures leads to enhancement in responsivityand decrement in PDCR.

Next, we demonstrate heterojunction of MoS_2 with conventional GaN for photodetector applications. The electrical characterization of the heterojunction shows diode like behavior. The interface properties were studied using Kelvin Probe Force Microscopy by surface potential mapping at the MoS_2/GaN heterojunction. The conduction band offset was also calculated. The origin of diode like behavior is attributed to unique type II band alignment of the heterojunction.

The photodetector parameters such as photoresponsivity and detectivity of the heterojunction were found to depend on power density of the incident light. High value of responsivity and detectivity depicts that the fabricated device can detect very low optical signal. Moreover, the device shows photoresponse in UV region also. These observations suggest that MoS_2/GaN heterojunction can have great potential for photodetection applications.

After *n-N* heterojunction investigation, MoS_2/*p*-GaN heterojunction was fabricated. The *P-n* heterojunction shows diode behavior with 3 orders of current rectification ratio. Ohmic contact fabrication on both MoS_2 and GaN reveals that the rectifying nature of the heterojunction stems from the interface. The as-fabricated diode is tested at high temperatures and it is observed that ideality factor improves with the increasing temperature. In addition, photoresponse characterizations reveal that the *P-n* heterojunction is highly sensitive to 405 nm laser. The heterojunction diode acts as self-powered photodetector. Our findings hold promise for heterojunction of MoS_2 with conventional semiconductor GaN in high efficient photodetector application.

सार

मोलिब्डेनम डाइसल्फ़ाइड (MoS_2), एक स्तरित धातु डाइक्लोजेनाइड ने अपनी परत पर निर्भर अद्वितीय गुणों के कारण नैनोइलेक्ट्रॉनिक्स में अपनी क्षमता दिखाई है। MoS_2 की अनूठी विशेषताओं में से एक है अप्रत्यक्ष से प्रत्यक्ष तक बैंडगैप परिवर्तन, जब परत की संख्या एकल परमाणु परत तक घट जाती है। MoS_2 पर आधारित विभिन्न इलेक्ट्रॉनिक उपकरणों का प्रदर्शन किया गया है जैसे कि FETs, फोटोडेटेक्टर्स, सेंसर, लचीले और पारदर्शी उपकरण आदि जो आधुनिक डिवाइस की दुनिया में इसकी क्षमता को दर्शाते हैं। इलेक्ट्रॉनिक उपकरणों का प्रदर्शन मुख्य रूप से धातु-अर्धचालक संपर्कों द्वारा नियंत्रित किया जाता है और डिवाइस के उचित कामकाज के लिए MoS_2 पर उच्च गुणवत्ता वाले विद्युत संपर्कों का निर्माण महत्वपूर्ण है। हमने MoS_2 पर इष्टतम विद्युत संपर्कों को निर्माण करने और इंटरफ़ेस पर प्रमुख विद्युत परिवहन तंत्र का निर्धारण करने को अपना पहला उद्देश्य निर्धारित किया है। MoS_2 के एकल परत समकक्ष को ध्यान में रखते हुए, इसकी प्रत्यक्ष बैंडगैप प्रकृति, अल्ट्राथिन फॉर्म में भी उच्च विद्युत प्रदर्शन की वजह से यह छोटे आकार के ऑप्टोइलेक्ट्रोनिक उपकरणों में अनुप्रयोगों के लिए उपयुक्त साबित होता है। हमारे दूसरे उद्देश्य के रूप में, हम एकल परत MoS_2 डिवाइस में फोटोडेटेक्शन घटना की जांच करने की कोशिश करते हैं। केवल MoS_2 पर आधारित उपकरणों के अलावा, अन्य पारंपरिक पदार्थों के साथ इसके उपयोग ने अनुसंधान का महत्वपूर्ण मात्रा में ध्यान आकर्षित किया है। स्तरित पदार्थों में वैन डेर वाल्स बलों का अस्तित्व हेटरोस्ट्रक्चर के विकास के लिए अन्य पारंपरिक तरीकों की तुलना में हेटरोस्ट्रक्चर के विभिन्न संयोजन को प्रदर्शित करने के खुले अवसर प्रदान करता है। इसके बाद, हम MoS_2 और गैलियम नाइट्राइड (GaN) पर आधारित हेटरोस्ट्रक्चर डिवाइस डिज़ाइन के प्रदर्शन का लक्ष्य रखते हैं। हेटेरोजंक्शन डिवाइस दोनों अर्धचालकों की कार्यक्षमता को बढ़ाते हैं और नए डिवाइस अनुप्रयोगों को जन्म दे सकते हैं।

काम के प्रारंभिक भाग में, विद्युत संपर्कों को यंत्रवत् एक्सफ़ोलीएटेड MoS_2 फ्लेक्स पर गढ़ा और चित्रित किया गया है। MoS_2 पर तुलनात्मक विद्युत अध्ययन विभिन्न धातुओं के साथ किया गया है और विद्युत प्रवाह-वोल्टेज विशेषताओं से पता चलता है कि चांदी निकल और क्रोमियम संपर्कों जैसे अन्य धातुओं की तुलना में I-V विशेषताओं में 100 गुना अधिक विद्युत प्रवाह और बेहतर रैखिकता और समरूपता दिखाती है। ओहमिक संपर्क के गठन की पुष्टि केवल विद्युत प्रवाह-वोल्टेज वक्र के रैखिक व्यवहार से नहीं की जा सकती। इसलिए,

MoS_2 पर Ag/Au संपर्कों का उपयोग करके ट्रांसमिशन लाइन मॉडल (TLM) लागू किया गया। विशिष्ट संपर्क प्रतिरोधकता को 4.54×10^{-4} Ω–cm^2 मापा गया। बैरियर की ऊँचाई और आईडीएलिटी फैक्टर 0.56 eV और 2.1, क्रमशः थर्मिओनिक उत्सर्जन करंट इक्वेशन का उपयोग करके प्राप्त किया गया है। अगले भाग में, माइक्रोस्कोपिक Pt/MoS_2 शोट्की डायोड के तापमान पर निर्भर विद्युत लक्षण प्रदर्शन किए गए थे। कमरे के तापमान से लेकर 80 K तक पूरे तापमान रेंज में रेक्टिफाइंग करंट-वोल्टेज विशेषताओं को प्राप्त किया गया। जैसे ही तापमान 296 K से घटकर 80 K हो जाता है, शोट्की बैरियर की ऊंचाई कम हो जाती है जबकि आईडीएलिटी फैक्टर बढ़ जाता है। बैरियर इनहोमोजेनिटी मॉडल के आधार पर शोट्की डायोड मापदंडों की तापमान निर्भरता को समझाया गया। शोट्की बाधा ऊंचाई के गॉसियन वितरण को मानते हुए, असमानता का स्तर तापमान क्षेत्रों 80 K से 140 K और 160 K से 296 K में क्रमशः 64 और 102 meV पाया गया। ये अवलोकन सूक्ष्मदर्शी उपकरणों में भी असमान शोट्की अवरोध को दर्शाते हैं।

बाद के काम में, एकल परत MoS_2 के ऑप्टोइलेक्ट्रोनिक प्रदर्शन का अध्ययन किया गया क्योंकि यह एक सीधा बैंडगैप सेमीकंडक्टर है। Pd/MoS_2/Pd मेटल-सेमीकंडक्टर-मेटल ज्योमेट्री को MoS_2 पर हाई बेरियर फोटोडेटेक्टर बनाने के लिए चुना गया था। बिजली के लक्षण वर्णन उच्च-शॉटकी अवरोध को प्रकट करते हैं जो Pd-MoS_2 इंटरफेस में मौजूद होते हैं जो कम गहरे प्रवाह की ओर जाता है। 650 nm लेजर के लिए 2 mW/cm^2 की शक्ति घनत्व पर 0.8 A/W की प्रतिक्रिया के साथ, डिवाइस रोशनी के बाद विद्युत प्रवाह में महत्वपूर्ण वृद्धि दिखाता है। घटना शक्ति घनत्व के साथ फोटोकरंट के रैखिक व्यवहार से MSM डिवाइस के प्रदर्शन पर ट्रैप स्टेट्स के कम प्रभाव का पता चलता है। जैसे-जैसे लेजर पावर घनत्व बढ़ता है, वैसे-वैसे रेस्पॉन्सिविटी भी बढ़ती जाती है। डिवाइस की स्थिरता की जांच करने के लिए उच्च तापमान पर डिवाइस के फोटोडेटेक्शन प्रदर्शन की भी जांच की गई। फैब्रिकेटेड डिवाइस के ऑप्टोइलेक्ट्रोनिक प्रदर्शन की जांच विद्युत प्रवाह माप द्वारा उच्च ऑपरेटिंग तापमान पर की गई थी। फोटोडेटेक्टर पैरामीटर जैसे फोटो से लेकर डार्क करंट रेशियो (PDCR) और रेस्पॉन्सिविटी को तापमान के साथ अलग-अलग देखा गया। PDCR में कमी देखी गई जबकि रेस्पॉन्सिविटी में तापमान के साथ वृद्धि देखी गई। डार्क करंट के साथ-साथ उच्च तापमान पर फोटो करंट की वृद्धि से PDCR में कमी होती है और रेस्पॉन्सिविटी में वृद्धि होती है।

अगले भाग में, हम फोटोडेटेक्टर अनुप्रयोगों के लिए पारंपरिक GaN के साथ MoS_2 के हेटेरोजंक्शन को प्रदर्शित करते हैं। हेटेरोजंक्शन का विद्युत लक्षण वर्णन डायोड की तरह व्यवहार को दर्शाता है। MoS_2/GaN हेटेरोजंक्शन पर सतह के संभावित मानचित्रण द्वारा केल्विन जांच बल माइक्रोस्कोपी का उपयोग करके

इंटरफ़ेस गुणों का अध्ययन किया गया। चालन बैंड ऑफसेट की भी गणना की गई। डायोड जैसे व्यवहार की उत्पत्ति को हेटेरोजंक्शन के अद्वितीय प्रकार II बैंड संरेखण के लिए जिम्मेदार ठहराया जाता है। फोटो रेस्पॉन्सिविटी और डिटेक्टीविटी जैसे फोटोडेटेक्टर पैरामीटर घटना प्रकाश की शक्ति घनत्व पर निर्भर करते पाए गए। रेस्पॉन्सिविटी और डिटेक्टीविटी का उच्च मूल्य दर्शाता है कि निर्मित डिवाइस बहुत कम ऑप्टिकल सिग्नल का पता लगा सकता है। इसके अलावा, डिवाइस यूवी क्षेत्र में भी फोटोरेस्पॉन्स दिखाता है। इन टिप्पणियों से पता चलता है कि MoS_2/GaN हेटेरोजंक्शन फोटोडेटेक्शन अनुप्रयोगों के लिए काफी संभावनाएं हो सकती हैं।

n-n हेटेरोजंक्शन जांच के बाद, MoS_2/p-GaN हेटेरोजंक्शन गढ़ा गया था। P-n हेटेरोजंक्शन 1000 विद्युत प्रवाह सुधार अनुपात के साथ डायोड व्यवहार को दर्शाता है। MoS_2 और GaN दोनों पर ओहमिक संपर्क निर्माण से पता चलता है कि हेटेरोजंक्शन की सुधारात्मक प्रकृति इंटरफ़ेस से उपजी है। उच्च तापमान पर गढ़े गए डायोड का परीक्षण किया गया और यह देखा गया कि बढ़ते तापमान के साथ आईडीएलिटी फैक्टर में सुधार होता है। इसके अलावा, फोटोरेस्पॉन्स लक्षण वर्णन से पता चलता है कि हेटेरोजंक्शन 405 nm लेजर के प्रति अत्यधिक संवेदनशील है। हेटेरोजंक्शन डायोड स्व-संचालित फोटोडेटेक्टर के रूप में कार्य करता है। हमारे निष्कर्ष उच्च कुशल फोटोडेटेक्टर अनुप्रयोग में पारंपरिक सेमीकंडक्टर GaN के साथ MoS_2 के हेटेरोजंक्शन की क्षमता दिखाते हैं।

Table of Contents

Certificate i

Acknowledgements ii

Abstract iv

Table of Contents vii

List of Figures xi

List of Tables xvii

List of Symbols and Abbreviations xviii

Chapter -1: Introduction……………………………………………………….…..1

1.1 Layered materials: An overview…………………………………………..…..……. 2

1.2 Molybdenum disulphide: A transition metal dichalcogenide……………………..…... 2

1.3 Electrical contacts to molybdenum disulphide……………...…………………..….. 4

1.3.1 Ohmic contacts…………………………………………………………….… 5

1.3.2 Transmission line model (TLM) measurements……………………………...… 7

1.3.3 Schottky contacts……………………………………………………………….. 8

1.4 Barrier inhomogeneity………………………………………………………………… 12

1.5 Photodetection in ultrathin 2D semiconductors……………………………………….. 13

1.6 Heterojunction of layered materials with conventional semiconductors……………… 15

1.7 Objectives of the thesis…………………………………………………….……… 17

1.8 Thesis organization……………………………………………………………………. 18

1.9 References…………………………………………………………………………….. 21

Chapter -2: Experimental techniques……………………………………………..28

2.1 Sample preparation ……………………………………….……………....……... 29

2.1.1 Sample cleaning……………………………………………………………… 29

2.1.2 Transfer of MoS_2 on other substrates………….……………………..…....... 29
2.1.2.1 Mechanical exfoliation method……………………………………….. 29
2.1.2.2 Chemical vapour deposition method………………………………….. 29
2.2 Fabrication techniques…………………………………………………….…... 30
2.2.1 Electron beam lithography…………………………………………...… 30
2.2.2 Thermal evaporation system…………………………………………. 32
2.2.3 Sputtering system……………………………………………………. 33
2.3 Characterization techniques ……………………………………………………... 33
2.3.1 Raman spectroscopy……….. …………………………….……………… 33
2.3.2 Photoluminescence (PL) measurements...……………………………….…… 33
2.3.3 Atomic Force Microscopy (AFM)……………………………………………. 34
2.3.4 Kelvin Probe Force Microscopy (KPFM)……………………………………… 34
2.3.5 Electrical characterization system……………………………………………… 35
2.3.6 Photodetection set up…………………………………………………………… 37
2.4 References……………………………………………………………………….. 39

Chapter -3: Study of Ohmic and Schottky contacts on MoS_2 and barrier inhomogeneity investigation in Schottky barrier diodes based on MoS_2 ……40

3.1 Introduction …………………………………….………………..…...…….. 41
3.2 Experimental section…………………………………….……………………. 42
3.3 Results and discussion……………………………………………...…………… 43
3.3.1 Characterization of exfoliated MoS_2 samples………………………………….. 43
3.3.2 Electrical characterization of different metal contacts to MoS_2……………….. 44
3.3.3 TLM investigation on MoS_2…………………………………………….……... 46
3.3.4 Electrical characterization of Pt/MoS_2 Schottky barrier diode ……………...… 48
3.3.5 Temperature dependent electrical characterization of Pt/MoS_2 Schottky diode 51
3.3.6 Barrier inhomogeneity at Pt/MoS_2 interface.........……………………………. 54
3.4 Conclusions………………………………………………………………………….. 58
3.5 References ………………. ……………………………………………………….... 59

Chapter -4: Study of the photoresponse behavior of high barrier Pd/MoS_2/Pd photodetector ……….……………………………………………………..….63

4.1 Introduction ……………………………………….………………..…...…….. 64
4.2 Experimental section……………………………………….…………………… 65
4.3 Results and discussion…………………………………………….....…………… 65
4.3.1 Electrical characterization of Pd-MoS_2-Pd MSM device.……………….……. 66
4.3.2 Photoresponse investigation of the device ……………...........…………….. 68
4.3.3 High temperature photodetection of the device ……..……….………………... 73
4.4 Conclusions…………………………………………..……………………….. 75
4.5 References ……………..…………………………………………………….... 76

Chapter -5: Fabrication and characterization of MoS_2/GaN heterojunction for photodetection applications...………….……………………………..……79

5.1 Introduction ……………………………………….………………..…...…….. 80
5.2 Experimental section……………………………………….…………………… 81
5.3 Results…………………………………………………………….....…………… 83
5.3.1 Electrical characterization of exfoliated MoS_2/*n*-GaN heterojunction ……..….. 83
5.3.2 Photoresponse properties of the heterojunction ………...........…………….. 86
5.3.3 KPFM investigation of the interface…………………...……………….…... 91
5.4 Discussion…………………………………………………………………….... 93
5.5 Conclusions……………………………..…………………………………….. 94
5.6 References ………………. ……………………………………………………... 96

Chapter -6: Electric and photoelectric behavior of *P-n* heterojunction based on gallium nitride and molybdenum disulfide..…..…………….………..……. …..100

6.1 Introduction ……………………………………….………………..…...…….. 101
6.2 Experimental section……………………………………….…………………… 102
6.3 Results and discussion.……………………………………………....…………… 103

6.3.1 Electrical characterization of MoS_2/GaN *n-P* heterojunction………………….….. 103
6.3.2 Temperature dependent electrical characterization of the heterojunction ……... 105
6.3.3 Photodetection properties of the *P-n* diode……………...…………………….…... 110
6.4 Conclusions………………………………..………………………………….. 112
6.5 References ………………. ………………………………………………………... 114

Chapter -7: Summary and future perspective ...….……………….…………...…116

7.1 Summary………...……………………………..………………...…...…….. 117
7.2 Future perspective……..………………………………….……………………. 119

List of publications..……………………………..……...……………...…...…….. 121
List of presentations in International/National Conferences..……………………….………. 121
Bio-data…………………………………………………………………...………. 124

List of Figures

Chapter – 1

Figure 1.1 A few applications of MoS_2 (a) Field effect transistor fabricated on MoS_2 with HfO_2 dielectric (b) Schematic representation of a MoS_2 based sensor for organic analytes (c) Flexible MoS_2 based device fabricated on flexible substrate (d) Optoelectronic device with a high-k Al_2O_3 dielectric and ITO as top gate…..……………………………………………………….……… **3**

Figure 1.2 Energy band diagram of metal-semiconductor (*n*-type) contact for Ohmic contact formation (a) before contact (b) after contact. E_{vac} is the reference vacuum level. ϕ_{metal} and ϕ_S are the work functions of contacting metal and semiconductor, respectively. χ is the electron affinity of the semiconductor and E_g is the bandgap. E_C, E_V, $E_{F,S}$ and $E_{F,metal}$ represent conduction band edge, valence band edge, Fermi level of semiconductor and Fermi level of metal, respectively………………………………………………………………… **5**

Figure 1.3 Different types of metal-semiconductor contacts (a) Schematic of a metal/bulk 3D semiconductor interface depicting covalent bonding between the metal and semiconductor (b) Metal/layered semiconductor interface with van der Waals gap between metal and semiconductor (e.g. Au-MoS_2 interface) (c) Metal/layered semiconductor interface with hybridization (e.g. Ti-MoS_2 interface, alloy is formed at the interface)…………………………... **6**

Figure 1.4 (a) Schematic diagram of Transmission line measurements. W represents the length of the contact pad, d_1, d_2…d_7 represent the distance between the consecutive electrodes (b) Plot of total resistance vs distance between electrodes. Slope and intercept of the fitted line gives sheet resistance and contact resistance, respectively…………………………………………….. **7**

Figure 1.5 Energy band diagram of metal-semiconductor (*n*-type) contact for Schottky contact formation (a) before contact (b) after contact. ϕ_B and V_{bi} represent the Schottky barrier height and built-in potential barrier, respectively…………… **9**

Figure 1.6 Current transport mechanism in metal-semiconductor Schottky contact (a) TE, TFE, FE represent thermionic emission, thermionic field emission and field emission processes, respectively (b) TAT represents trap assisted tunneling……………………………………………………………………… **10**

Figure 1.7 Schottky barrier height of different metals with MoS_2 as reported in the literature………………………………..……………………………….. **11**

Figure 1.8 Energy band diagram of Schottky contact showing inhomogeneous metal-semiconductor interface………………………………………………………… **12**
Figure 1.9 Absorbance spectra of monolayer MoS_2 showing absorption peaks corresponding to A and B excitons as observed by UV-vis spectrophotometer. **14**

Chapter – 2

Figure 2.1 Raith eLine plus EBL system installed at Nanoscale Research Facility Centre at IIT Delhi, India…………………………………..…………………….... **31**
Figure 2.2 Keithley semiconductor characterization system and EverBeing DC Probe station at Nanoscale Research Facility Centre at IIT Delhi…………………… **35**
Figure 2.3 Photograph of the dipstick cryostat designed for variable temperature electrical measurements………………..……………………………… **37**
Figure 2.4 Photodetection setup installed at the Nanoscale Research Facility Centre at IIT Delhi………………………………………………………………… **38**

Chapter – 3

Figure 3.1 (a) Raman spectra of exfoliated multilayer MoS_2 flake showing both in-plane (E^1_{2g}) and out-of-plane (A_{1g}) vibrational modes (b) Height profile of the flake showing thickness of 25 nm……………………………………………….. **44**
Figure 3.2 SEM images of the metal-MoS_2 contacts: (a) Cr-MoS_2-Cr (b) Ni-MoS_2-Ni (c) Ag-MoS_2-Ag. Current-voltage measurements of the metal contacts on MoS_2 flake: (d) linear plot (e) Semilog plot showing significant change in current in case of Ag-MoS_2 contact (Representation of Ni contacts in red color, Cr in black color and Ag in blue color)……………………………… **45**
Figure 3.3 (a) Schematic diagram of TLM geometry (b) Optical image of the fabricated TLM pattern (c) SEM image of the fabricated TLM pattern…………………. **47**
Figure 3.4 (a) Current-voltage measurements of the Ag/Au contacts on MoS_2 flake for TLM geometry.(b) Plot of total resistance vs channel length used to extract contact resistance ($2R_C$ = y-intercept) and sheet resistance (slope)…………... **48**
Figure 3.5 (a) 3D schematic representation of Pt/MoS_2 Schottky diode (b) Optical image of the Pt/MoS_2 Schottky barrier diode with Ag as Ohmic contact……………. **48**
Figure 3.6 Electrical characterization of platinum Schottky diode on MoS_2 flake taking silver as Ohmic contact (semilog plot showing clear current rectification) Inset shows the linear plot……………………………………………………. **49**

Figure 3.7 Schematic illustration of Energy Band diagram (a) before contact, χ, ϕ_s, E_c, E_v, E_F and E_{vac} represents the electron affinity, work function, conduction band edge, valence band edge, Fermi level of MoS_2 and vacuum level respectively. (b) Band diagram after contact showing band bending. One contact is the low barrier Ag contact and other is the high barrier Pt contact. ϕ_B shows the barrier height at Pt-MoS_2 side………………………………… **51**

Figure 3.8 (a) Semi log current-voltage characteristics of Pt/MoS_2 Schottky diode at different temperatures ranging from 80 K to 296 K at a step of 20 K (b) I-V-T curve in reverse bias case (c) I-V-T curve in forward bias case…………… **52**

Figure 3.9 Variation of (a) ideality factor and apparent barrier height with temperature (b) reverse leakage current with temperature for Pt/MoS_2 Schottky diode….. **53**

Figure 3.10 Variation of ϕ_{bo} with $(2kT)^{-1}$. Graph shows two linear regions in the temperature range 80 K to 140 K and 160 K to 296 K……………………….. **54**

Figure 3.11 Modified activation energy plot vs $(kT)^{-1}$, giving value of Richardson constant 102 $A/(cm\text{-}K)^2$ in the temperature range 160 K to 296 K and 85 $A/(cm\text{-}K)^2$ in the temperature range 80 K to 140 K………………………... **55**

Figure 3.12 Schematic representation of band diagram of Pt-MoS_2 Schottky contact (a) before contact (b) after contact (c) 3D representation of inhomogeneous barrier. E_C, E_F, E_V represents conduction band edge, Fermi level and valence band edge, respectively. χ and ϕ_B represent electron affinity and barrier height, respectively……………………………………………………... **57**

Chapter – 4

Figure 4.1 (a) Raman spectra of CVD grown monolayer MoS_2 showing the difference between dominant Raman peaks to be 20 cm^{-1} (b) Photoluminescence spectra of monolayer MoS_2 (c) AFM image of monolayer MoS_2 flake on SiO_2 substrate………………………………………………………. **66**

Figure 4.2 (a) Schematic diagram of the MSM device (b) Optical image of the device…. **66**

Figure 4.3 Plot of ln[Iexp(eV/kT)] vs V for Pd-MoS_2-Pd MSM structure in dark condition for calculation of ideality factor and barrier height. Inset shows the log plot of dark I-V characteristics Schematic diagram of the MSM device…. **68**

Figure 4.4 I-V characteristics of the device under dark and illumination conditions with wavelength 650 nm (power density: 1mW/cm^2)…………………………….. **69**

Figure 4.5 (a) Plot of responsivity with the power density of incident light (wavelength: 650 nm) at a bias voltage of -1 V (b) Plot of photocurrent with power density showing linear behavior…………………………………………………... **70**

Figure 4.6 Spectral response of the MSM device at a broad range of wavelengths ranging from UV to NIR…………………………………………………….. **71**

Figure 4.7 Absorbance spectra of monolayer MoS_2 showing B and A exciton peaks at 612 nm (2.02 eV) and 664 nm (1.86 eV), respectively……………………… **72**

Figure 4.8 (a) I-V characteristics of the device at different intervals of illumination time (b) Temporal response of the device……………………………………... **72**

Figure 4.9 Semilog I-V characteristics of the device at different temperatures………… **74**

Figure 4.10 (a) Plot of dark current density and measured PDCR of the MSM device with the temperature at a bias voltage of 1V (b) Behavior of photoresponsivity with increasing temperature (Bias voltage: 1V). All the current measurements with laser were performed just after illumination…………… **74**

Chapter – 5

Figure 5.1 Process flow of the fabrication process (a) GaN/Sapphire substrate (b) Transfer of MoS_2 flakes on GaN/Sapphire substrate (c) Deposition of SiO_2 on the template for insulation of electrodes (d) Selective etching of SiO_2 over MoS_2 and GaN (e) Electrode deposition on MoS_2 and GaN ……………… **82**

Figure 5.2 (a) Raman spectra of exfoliated MoS_2 flake taken using 532 nm laser indicating in plane E^1_{2g} and out of plane A_{1g} raman mode (b) AFM image of the exfoliated flake…………………...……………………………….. **83**

Figure 5.3 Fabrication of Ohmic contact to *n*-GaN (a) Schematic diagram of metal contacts to n-GaN (b) Current–voltage characteristics of Ohmic contacts to *n*-GaN. I-V curve shows the Ohmic behavior of *n*-GaN with Cr/Au (5nm/50nm) contacts……………………………….......................... **84**

Figure 5.4 Fabrication of metal contacts to MoS_2 flake a) SEM image of fabricated Cr/Au (5nm/50nm) contacts on MoS_2 flake fabricated using e-beam lithography b) Electrical characterization of Au/Cr/MoS_2 showing nearly Ohmic behavior……………………………………………………………… **84**

Figure 5.5 (a) 3D Schematic illustration of MoS_2/GaN heterojunction device (b) Optical microscope image of the fabricated heterojunction with Cr/Au (5nm/50nm) contacts (c) Two terminal electrical measurements of the MoS_2/GaN heterojunction diode under dark conditions showing clear current rectification………………………………………………………………. **85**

Figure 5.6 Photoresponse of MoS_2/GaN heterojunction under illumination with 405 nm laser (a) Linear plot of photoinduced behavior of MoS_2/GaN heterojunction under different illumination intensities of 405 nm laser source (b) Plots of responsivity and detectivity with light intensity (c) Photoelectrical behavior of device under illumination of 650 nm and 405 nm laser (d) log plot of electrical behavior of the device after exposure to UV light (365 nm)…….. **87**

Figure 5.7 Photocurrent of the MoS_2/GaN heterojunction under illumination with 405 nm laser as a function of power density. The inset figure shows the linear plot…….. **89**

Figure 5.8 (a) Time dependence of photocurrent of the MoS_2/GaN heterojunction observed by illumination via laser light (405 nm) at a bias of 5V with fixed illumination intensity of 12 mW/cm^2 (b) Magnified plot of one response cycle (c) Exponential curve fitting of the rise showing fast rise time and slow rise time (d) Exponential curve fitting of the decay showing fast decay time followed by slow decay (On and off represents the status when laser is on and off, respectively)……………………..…………………………………. **90**

Figure 5.9 (a) Kelvin Probe Force Microscope (KPFM) image of MoS_2 flake on n-GaN showing change in surface potential between MoS_2 and GaN (b) Plot of surface potential difference with lateral distance across MoS_2/GaN interface along the line as indicated in (a)……………………………………..….. **91**

Figure 5.10 Energy band diagram of the heterojunction (a) After contact (zero bias) (b) Forward bias (negative bias is given to MoS_2 with respect to GaN) (c) Forward bias under photoexcitation with laser wavelength 405 nm. E_C, E_V, E_F and E_{vac} represent bottom of conduction band, top of valence band, Fermi level and vacuum level, respectively. Band gap of MoS_2 and GaN is 1.2 eV and 3.4 eV, respectively. ΔE_C represents the conduction band offset……… **94**

Chapter – 6

Figure 6.1 Process flow of the fabrication process (a) *p*-GaN/Sapphire substrate (b) Ohmic contact formation on *p*-GaN using shadow masking (c) Transfer of MoS_2 flakes on *p*-GaN/Sapphire substrate (d) Hardening of PMMA on edge of MoS_2 flake for insulation of electrodes (e) electrode formation on MoS_2 (f) final device…………………………………………………………... **103**

Figure 6.2 Current-voltage characteristics of Ohmic contacts on (a) *p*-GaN using Ni/Au contacts (b) MoS_2 flake using Ag/Au contacts. Inset shows the schematic representation of the Ohmic contacts……………………………………… **104**

Figure 6.3 Optical image of the fabricated MoS_2/GaN *n-P* diode. The top electrode on MoS_2 is separated from the underneath substrate by an insulating PMMA layer…………………………………………………………………...... **104**

Figure 6.4 Electrical characterization of the MoS_2/GaN *n-P* heterojunction diode. (a) Output characteristics at room temperature exhibiting 3 orders of rectification. The top electrode contacted with the MoS_2 is grounded and the

	bias is applied on the electrode contacted with GaN film. (b) Semi-logarithmic plot of the curve………………………………………………….	**105**
Figure 6.5	Current-voltage characteristics of *P-n* heterojunction diode at various temperatures ranging from RT to 373 K **(a)** Linear plot **(b)** Log plot………..	**106**
Figure 6.6	The behavior of preexponential factor with temperature in region I for the *P-n* diode…………………………………………………………………….	**107**
Figure 6.7	Temperature dependence of Ideality factor…………………………………...	**108**
Figure 6.8	(a) Saturation current with temperature (b) plot of log I_s vs 1/kT. Slope of the line gives value of activation energy…………………………………………	**108**
Figure 6.9	Current vs applied voltage for reverse bias case at room temperature. Inset shows the I-V curve at low reverse bias………………………………………	**109**
Figure 6.10	Photoresponse of the MoS_2/GaN *n-P* heterojunction diode. (a) Semi-logarithmic output curves at various intensities of incident light at room temperature. External bias was applied on the electrode in contact with GaN and electrode in contact with MoS_2 was grounded (b) Dependence of photocurrent on power density at zero bias…………………………………..	**110**
Figure 6.11	The behavior of photo-responsivity with voltage at incident power density of 76 μW/cm^2………..………………………………………………………….	**111**
Figure 6.12	Time response of the device (a) At 0 bias (b) At 2V bias with incident laser intensity of 1 mW/cm^2………………………………………………………..	**112**

List of Tables

Chapter-3

Table 3.1 Values of apparent SBH, ideality factor and reverse leakage current for Pt/MoS_2 Schottky diode at different temperatures………………………….. **53**

Chapter-5

Table 5.1 Performance comparison of our MoS_2/GaN heterojunction based photodetector with other MoS_2 based photodetectors ..…………………….. **88**

List of Symbols and Abbreviations

Symbols

α	Absorption coefficient
A	Effective area of the device
$A*$	Richardson's constant
d	Distance between electrodes in TLM pattern
D	Detectivity
e	Electron charge
ε_n	Dielectric constant of MoS_2
ε_N	Dielectric constant of GaN
E_g	Bandgap of the semiconductor
G	Gain in the device
h	Planck's constant
I_{ph}	Photocurrent
I_{dark}	Dark current
$I_{illuminated}$	Current after illumination
I_S	Saturation current
J	Current density
k	Boltzmann's constant
L	Length of the device
L_T	Transfer length
$m^*_{MoS_2}$	Effective mass of electron in MoS_2
m^*_{GaN}	Effective mass of electron in GaN
$P_{illuminated}$	Illuminated power
P_{abs}	Absorbed power
P_{in}	Incident power
R	Responsivity
R_T	Total resistance of the device
R_C	Contact resistance
R_{sheet}	Sheet resistance
T	Absolute temperature
t_{life}	Lifetime of the carriers
$t_{transit}$	Transit time
V_{bi}	Built-in potential
W	Length of the electrode
x_n	Depletion width in MoS_2 side
x_N	Depletion width in GaN side
ϕ_{metal}	Work function of the metal
ϕ_S	Work function of the semiconductor

ϕ_B	Schottky barrier height
ϕ_{tip}	Work function of the tip
ϕ_{GaN}	Work function of GaN
ϕ_{MoS_2}	Work function of MoS_2
ϕ_{bl}	Local barrier height
ϕ_{bo}	Zero bias barrier height
$\overline{\phi_{bo}}$	Mean barrier height
η	Ideality factor
χ	Electron affinity of the semiconductor
μ	Mobility
σ_S	Standard deviation of the Gaussian distribution of Schottky barrier height
ΔE_C	Conduction band offset

Abbreviations

AFM	Atomic Force Microscopy
CVD	Chemical Vapor Deposition
CAFM	Conducting Atomic Force Microscopy
CPD	Contact Potential Difference
DI	Deionized
DUT	Device under test
EBL	Electron Beam Lithography
FE	Field Emission
FETs	Field Effect Transistors
FLP	Fermi Level Pinning
GaN	Gallium Nitride
HF	Hydrofluoric acid
I-V	Current-Voltage
I-t	Current-Time
IF	Ideality Factor
KPFM	Kelvin Probe Force Microscopy
LEDs	Light Emitting Diodes
MOVPE	Metal Organic Vapor Phase Epitaxy
MoS_2	Molybdenum Disulfide
MSM	Metal-Semiconductor-Metal
NIR	Near-infrared
PL	Photoluminescence
PMMA	Poly Methyl Meth-Acrylate
PDCR	Photo-to-dark current ratio
RT	Room Temperature
RTA	Rapid Thermal Annealing
SBH	Schottky Barrier Height
SiO_2	Silicon dioxide

SMU	Source measuring unit
SCS	Semiconductor Characterization System
TMDCs	Transition Metal Dichalcogenides
TLM	Transmission Line Model
TE	Thermionic Emission
TFE	Thermionic Field Emission
TAT	Trap Assisted Tunneling
UV	Ultraviolet
2D	Two-dimensional
3D	Three-dimensional